Biomedicine & Pharmacotherapy 83 (2016) 1203–1211

Available online at
ScienceDirect
www.sciencedirect.com

Elsevier Masson France
EM|consulte
www.em-consulte.com/en

Three dimensional tubular structure self-assembled by vascular mesenchymal cells at stiffness interfaces of hydrogels

Xiaolu Zhu, PhD[a,b,*], Shiva Gojgini[c], Ting-Hsuan Chen[d], Fang Teng[e], Peng Fei[b], Siyan Dong[b], Tatiana Segura[c], Chih-Ming Ho[b,f]

[a] School of Mechanical and Electrical Engineering, Hohai University, Changzhou, Jiangsu 213022, China
[b] Mechanical and Aerospace Engineering Department, University of California, Los Angeles, CA 90095, USA
[c] Chemical and Biomolecular Engineering Department, University of California, Los Angeles, CA 90095, USA
[d] Department of Mechanical and Biomedical Engineering, City University of Hong Kong, Hong Kong
[e] Department of Gynaecology and Obstetrics, Nanjing Maternity and Child Health Care Hospital Affiliated to Nanjing Medical University, Nanjing, China
[f] Bioengineering Department, University of California Los Angeles, Los Angeles, CA 90095, USA

ARTICLE INFO

Article history:
Received 19 May 2016
Received in revised form 26 July 2016
Accepted 8 August 2016

Keywords:
Self-organization
Hyaluronic acid
Turing instability
Mesenchymal stem cell

ABSTRACT

In this study, we report a rational and robust methodology to construct three dimensional (3D) tubular-structures solely by self-assembly of vascular mesenchymal cells (VMCs). Using the cell-laden hyaluronic acid hydrogel surrounded by cell-free gel with a higher stiffness, VMCs spontaneously migrated across the interface and assembled into 3D tubes, which composes of numerous cells. Based on turing instability which describes the reaction-diffusion processes of inhibitors and activators, this result of 3D tubular structure formation agrees with theoretical predictions from simulations of the reaction-diffusion of morphogens and cells under the initial conditions of patterned cell-laden hydrogel. We showed that this combination of theoretical prediction and experiments is able to produce multi-cellular 3D tubes with desired dimensions and determinate orientation in hydrogel mimicking the 3D features of tubular tissue. This work provides a reliable methodology for creating tubular structures with controllable sizes inside the 3D hydrogel through multi-cellular self-organization.

1. Introduction

Regenerative medicine uses a variety of cell/biomaterial-based approaches to repair and regenerate diseased or damaged tissues and organs [1,2]. Tubular structures are fundamental units in most organs. For example, the lung, kidney and vasculature are composed primarily of tubes [3], such as trachea, arteries, and lymph vessels. Therefore, artificially constructing tubular structures is urgently needed for advancing regenerative medicine. Recently, researchers use a stress-induced rolling membrane technique to fabricate tubular structures with configurable sizes [4]. This method can obtain micro-tubes with multi-layers consisting of different types of cells. However, the geometrical features, such as the diameters and wall thicknesses, are limited by the membrane thickness and number of rolling layers, creating obstacles to constructing smaller and thinner-wall tubular structure. A tubular structure can also form with a monolayer of cells along the fibrous direction in a micro-fibre shaped construct consisting of human umbilical vein endothelial cell (HUVEC) and collagen [5]. This is a typical scaffold-based approach yet with a deformable fibre as the scaffold. Moreover, 3D printing can produce networks of carbohydrate glass serving ascyto-compatible sacrificial scaffold to construct vascular architectures [6]. The hollow cellular structures can also be constructed by 3D bio-printer using the bio-mimetic components made of biomaterials, such as hydrogels encapulating cells [7]. Nevertheless, using structured scaffolds or hydrogel to “mold” 3D tubular structure or networks still pose concerns considering the bio-compatibility for many polymer materials or the structural complexity achievable. Moreover, artificially-predefined patterns at initial times are usually disorganized by cellular self-organization, such as cellular alignment or migrations, in the subsequent tissue development, creating uncertainly for those artificial attempts.

* Corresponding author at: School of Mechanical and Electrical Engineering, Hohai University, 200 North Jinling Road, Changzhou, Jiangsu 213022, China.
E-mail address: zhuxxiaoluu@yeah.net (X. Zhu).

http://dx.doi.org/10.1016/j.biopha.2016.08.018
0753-3322/

In addition to the methods based on scaffold with external guidance, the incorporation of self-organization in 3D culture is receiving increased attention for tissue regeneration [8,9]. Tubular structures were created by 3D cultures using a specific designed airway epithelial cell line and HUVECs under specifically tailored conditions [10]. Recently, researchers have created tubular vessel networks via cellular self-organization by co-culture of hepatic endoderm cells, HUVECs and human mesenchymal stem cells [9]. The vessel-like tube structure formation can be achieved by co-culture of outgrowth endothelial cells and adipose-derived stem cells in a fibrin matrix [11]. Yet, it has been challenging to regenerate tubular structures with diameters of hundreds of microns by self-organization of cells in 3D hydrogel. Due to the fact that they need an extraordinary complicated process and orchestration of various chemical, physical and mechanical cues in the microenvironment filled with a huge number of cells. More importantly, the appearance of these structural morphologies in complex biological systems is often not strategically planned or based on a controllable engineering approach, due to the lack of insights in the underlying mechanism. So far, there is rarely a rational and reliable methodology provided for creating 3D self-organized tubular structures with designed geometry and sizes.

Here we devised a solution to generate 3D multi-cellular tubes by utilizing multi-cellular self-organization. Using cell-laden hyaluronic acid (HA) hydrogel and cell-free hydrogel with higher stiffness, we found that VMCs can spontaneously assemble into 3D tubular structure tubes composed of numerous cells. The structure formation is mediated by the gradients of morphogen and cell concentrations arising from the structural interfaces of hydrogel stiffness. More importantly, the process presents intriguing agreement with theoretical predictions from simulations of the reaction-diffusion of morphogens described by turing instability as shown in our recent simulation work [12], providing a method for strategically planned or controllable engineering approach for tissue reconstruction. Mimicking the 3D features of tubular tissues with insights of underlying mechanism, our method has great potential for promoting the regenerative medicine to a new state with rationally controllable methodology.

2. Materials and methods

2.1. Cell culture

Vascular mesenchymal cells (VMCs) were isolated and cultured as previously described [13–16,23]. The cells were grown in Dulbecco's Modified Eagle's Medium (Invitrogen, CA, USA) supplemented with 15% heat-inactivated fetal bovine serum and 1% penicillin/streptomycin (10,000 I.U./10,000 μg/mL; all from Mediatech, VA, USA). Cells were incubated at 37 °C in a humidified incubator (5% CO_2 and 95% air) and sub-cultured every 3 days.

2.2. HA modification

Acrylated hyaluronic acid (HA-AC) was prepared using a two-step synthesis process [18,19]. HA (60 kDa, 1.0 g, 0.017 mmol) was reacted with 18.0 g (105.5 mmole) adipicdi hydrazide (ADH) at a pH of 4.75 in the presence of 1-ethyl-3-[3-dimethylaminopropyl] carbodi imide hydrochloride (EDC,2.0 g, 10.41 mmole) overnight and purified through dialysis (6000-8000 MWCO) in DI water for 1 week with changing water frequently. The purified intermediate (HA-ADH) was lyophilized and stored at −20 °C until used. Modified HA-ADH (1.0 g, 0.014 mmole) was reacted with N-Acryloxy succinimide (NHS-AC) (0.75 g, 4.4 mmole) in 4-(2-hydroxyethyl)-1-piperazine ethane-sulfonic acid (HEPES) buffer (pH 7.2) overnight and purified through dialysis in DI water for 1 week before lyophilization. The final product was analyzed with 1H NMR (D_2O) and the degree of acrylation (12%) was determined by dividing the multi-plet peak at $\delta = 6.2$ (cis and trans acrylate hydrogens) by the singlet peak at $\delta = 1.6$ (singlet peak of acetylmethyl protons in HA).

2.3. HA hydrogel formation

HA hydrogels were formed using Michael Addition chemistry between bis-cysteine containing MMP-degradable cross linker onto HA-AC pre-functionalized with cell adhesion peptides (RGD). A lyophilized HA-AC aliquot (6 mg) was dissolve in 75 μL of 0.3 M TEOA buffer. Lyophilized aliquots of the RGD peptides (0.1 mg/vial) were dissolved in TEOA buffer and mixed with HA–AC solution, and finally kept for reacting for 25 min at 37 °C to get the HA–RGD solution. The cells were split from the petri dish bottom by 0.25% trypsin-EDTA, and the resuspended cell solution was placed on ice. A lyophilized aliquot of the cross-linker (1.0 mg) was then diluted in 20 μL of 0.3 M TEOA buffer (pH = 8.4) immediately before mixing with HA–AC solution, HA-RGD (final concentration of 100–150 μM RGD), and the cell solution (3000–7500 cells per μL of final gel volume). The gel precursor solution was pipetted onto a sigmacoted glass slide in drop-wise (30–45 μL), then clamped with another sigmacoted slide with plastic cover-slip spacers, and finally incubated for 30 min at 37 °C to allow for gelation. The final

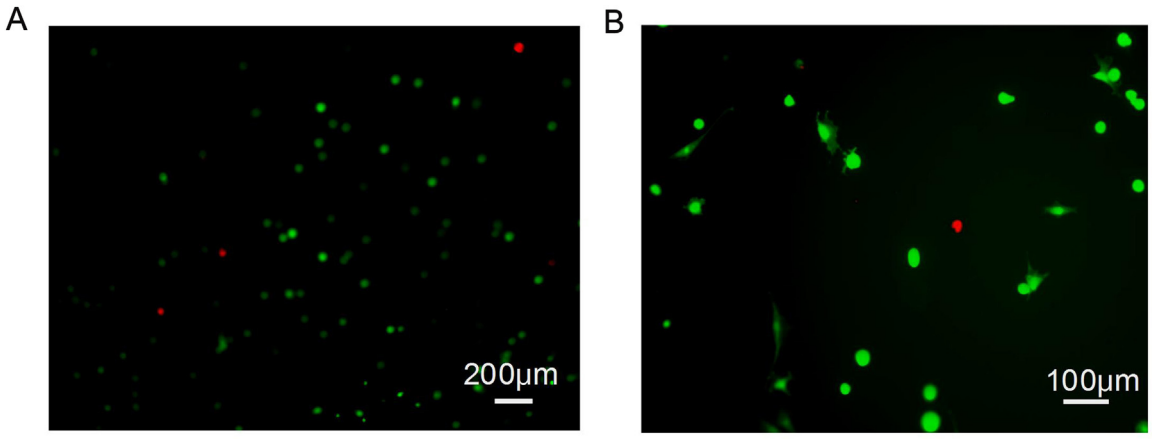

Fig. 1. The cell viability inside our modified HA hydrogels were studied using the LIVE/DEAD assay at day 1. (A) Magnification, the bar represents 200 μm. (B) Magnification, the bar represents 100 μm. The green represents the live cell. The red represents the dead cell.

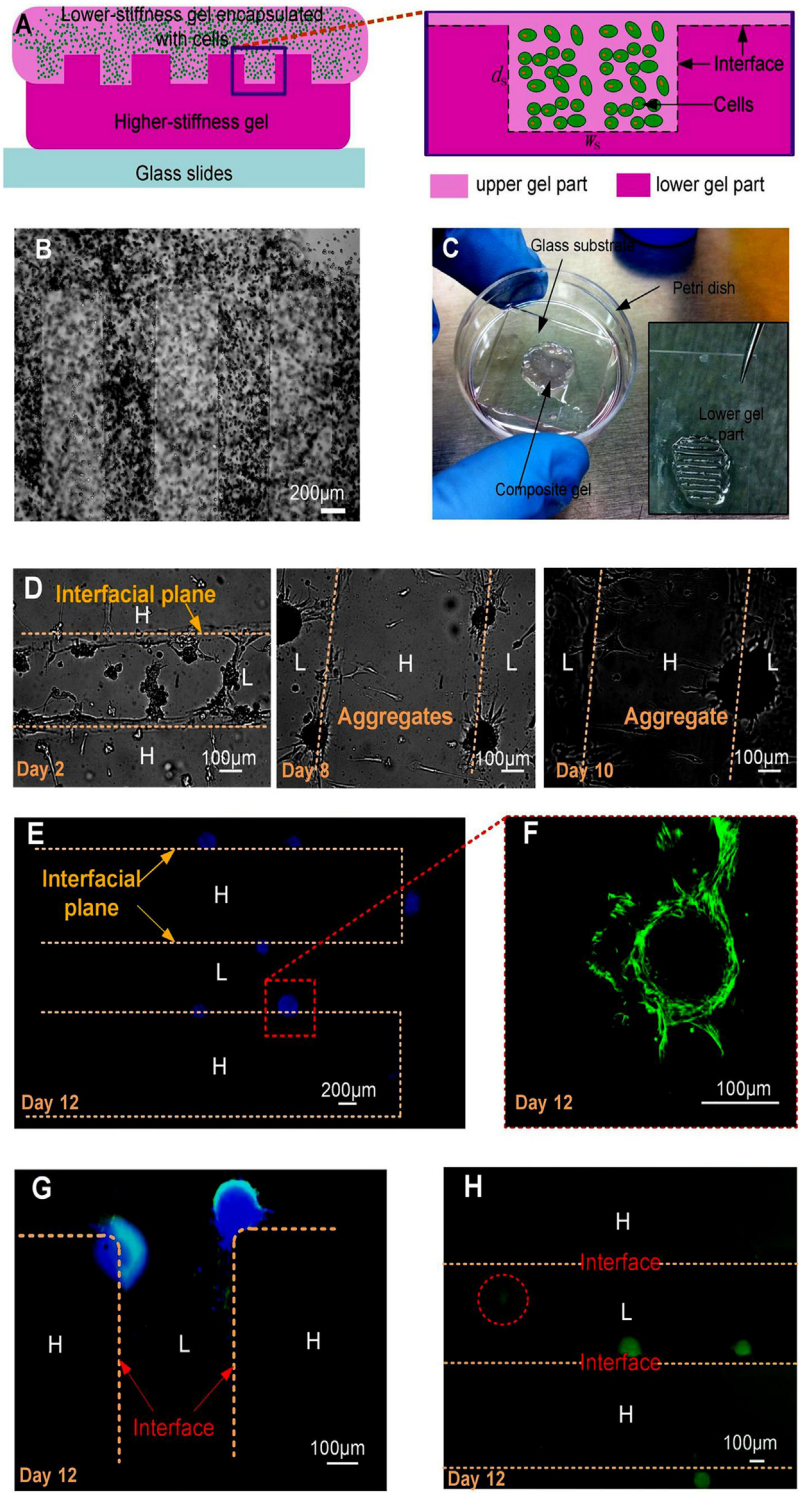

Fig. 2. Schematic design and experimental results of large-scale cellular self-organization inside 3D HA-hydrogel. (A) Schematic of the composite gels consisting of two parts of gels with a serrated interface between them. The cells were only encapsulated in the upper gel having lower stiffness. The green dots denote the cells. (B) Bright-field microscopy image showing patterned hydrogels with encapsulated cells in the lower stiffness gel part at initial time. (C) Composite gel attached on the slide in a 35-mm petri dish (inset: lower gel part in (A)). (D) Bright-field microscopy images at the interfacial of the upper and lower gel parts (Day 2 to Day 10). The character "H" and "L" indicate the hydrogel areas with higher and lower-stifness, respectively. (E) Fluorescence microscopy showing the top view of the self-formed multi-cellular structure at different locations dispersed along the interfacial planes. The aggregated blue dots were stained with DAPI. (F) Confocal laser-scanning microscopy showing the cross-section of the multi-cellular structure at the middle position in length direction, where green color represents the distribution of cellular F-actins. The multi-cellular structure appeared as hollow shape. (G and H) Fluorescence microscopy showing the top view of the self-formed multi-cellular structure in other locations. The tubes usually emerged around the straight interface. However, they can also be found in the vicinity of the corners (G) and the interior region (circled area) of the lower-stiffness gel (H).

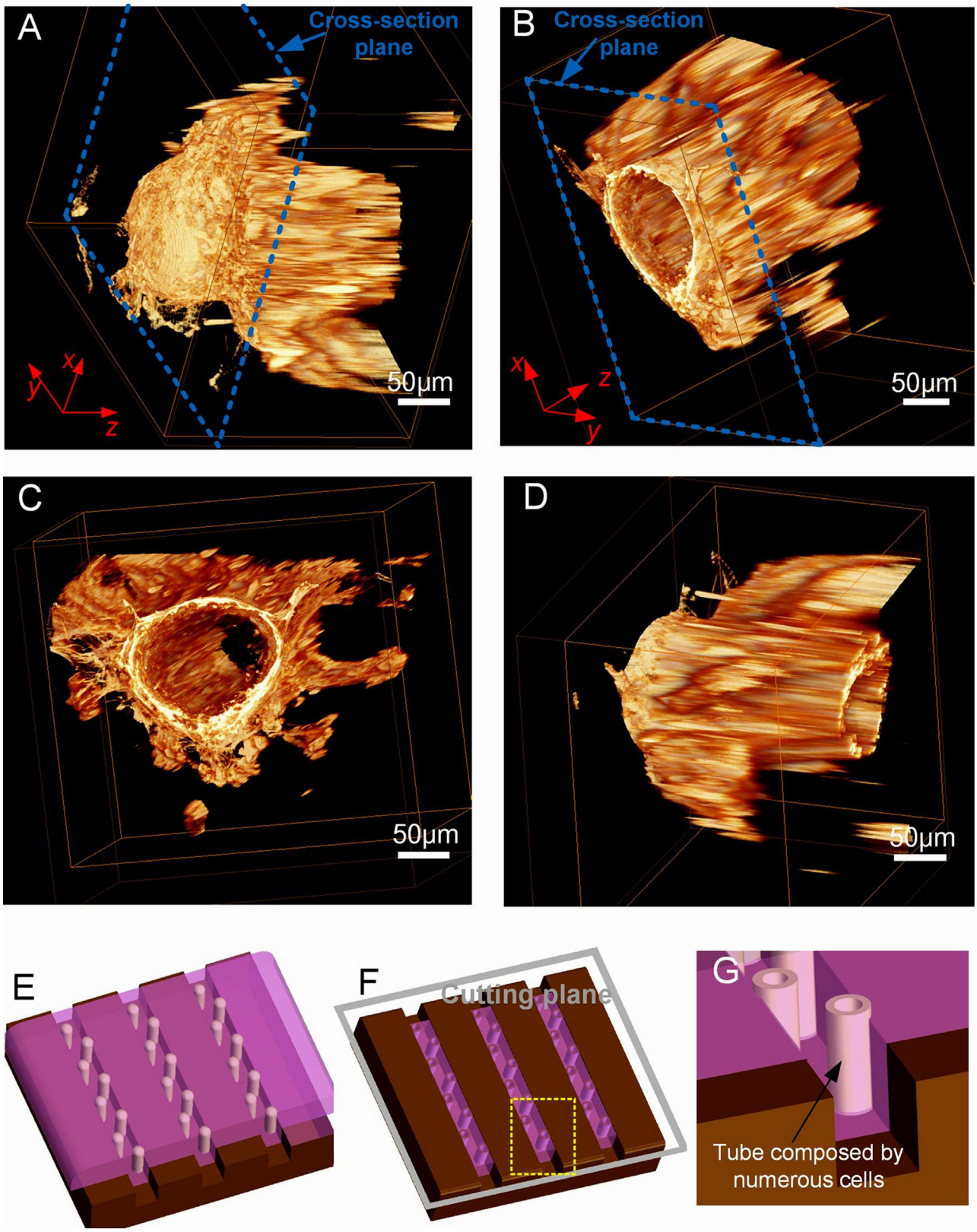

Fig. 3. 3D morphology of the hollow tubular structures by large-scale cellular self-organization inside 3DHA-hydrogel. (A and B) Confocal laser-scanning microscopy showing 3D reconstructed images of multi-cellular tube structure that had been cultured in HA hydrogel for 12 days. The revealed lumen of the tube presented by moving the cross-section plane toward right. (C and D) Top and side views of the multi-cellular structure in (B). (E) Generic drawing approximately presenting distribution of the formed tubes with dome shaped lids around the straight interface. (F) The part below the cutting plane in (E), which shows the lumen inside the tubes. (G) Schematic drawing for the magnified view of the detailed feature of hollow tubes formed around the interfaces. The "cap" at the end of tube was cut away for clarity of the inside hollow regions.

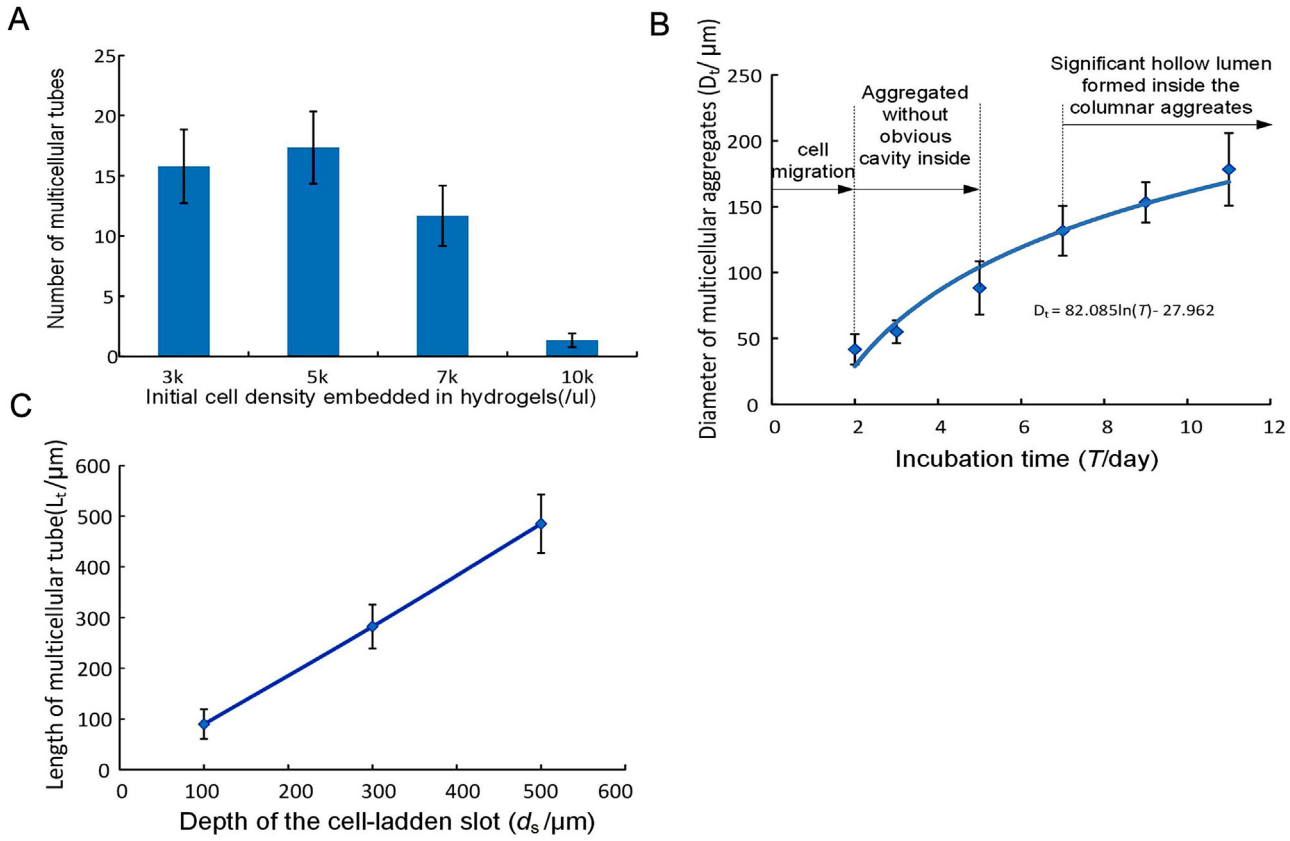

Fig. 4. Quantitative characterization of the tube formation in this cell-laden composite hydrogel system. (A) The number of tubes versus the initial cell density (mean ± standard deviation; n = 5). (B) The radial dimensions of the multi-cellular aggregates versus incubation time (mean ± standard deviation; n = 5) with an initial cell density of 5000 per μl. (C) Dependence of the tube length on the depth of cell-ladden slot in composite hydrogels with the initial cell density of 5000 per μl (mean ± standard deviation; n = 6).

gel was swelled in culture media before being placed inside 96-well plates for the following long-term culture. The mechanical properties of the hydrogels can be controlled by varying the HA concentration or the cross linking density, "r", which is defined as mole ratio of thiol (—SH) from the cross linkers toacrylate group (—ACs) from the HA–ACs.

2.4. Rheology measurement for charactering stiffness of hydrogels

The storage (G′) and loss modulus (G″) were measured with a plate-to-plate rheometer (Physica MCR, Anton Paar, Ashland, VA) using a 8 mm plate under a constant strain of 0.05 and frequency ranging from 0.1 rad/s to 10 rad/s. Hydrogels were made as detailed above and cut to a size of 8.0 mm in diameter to fit the plate. A humid hood was used to prevent the hydrogel from drying and the temperature was kept at 25 °C.

2.5. Fabrication of the composite hydrogel

The composite hydrogel consists of two subparts differing in their stiffness and has geometric interfaces between those two subparts. The main procedures for fabrication of the composite hydrogel are illustrated as the followings. Firstly, with a SU-8 master, which was prepared by standard photolithography process on a silicon wafer, a PDMS mold with serrated patterns was casted using a weight ratio of 10:1 for the base and curing agent and cured at 85 °C for 4 h. Based on the PDMS mold treated with oxygen plasma, a grooved hydrogel sheet with higher stiffness was casted, and the PDMS mold was removed from Gel-1 when they were immersed in PBS. Next, the precursor of Gel-2 encapsulating cells was placed on the patterned Gel-1, and a hydrophilic cover-slip was gently put on the top of Gel-2, followed by an incubation of the whole set for 30 min at 37 °C for gelation. At last, the cover slip and spacers were slightly detached after gelation, and then the composite gel with glass substrate was placed into a 35-mm petri dish filled with culture media.

2.6. Cytotoxicity test

In this study, the cell viability in these hydrogels was studied by using LIVE/DEAD viability/cytotoxicity kit (Molecular Probes, Eugene, OR). Briefly, 2 μL (1.8 μL) of ethidium homodimer-1 and 0.5 μL (0.7 μL) of calcein AM from the kit were diluted with 1 mL of DMEM. Each gel was stained with 150 μL of this staining solution for 30 min at 37° in the dark.

2.7. Immunofluorescence staining

Before fixation, the gel samples were washed two times with pre-warmed phosphate buffered saline (PBS). Then the cells in gel were fixed by 4% paraformaldehyde (PFA) solution for 40 min at room temperature. After that, the samples were washed 2–3 times with PBS, treated with 0.1% Triton X-100 in PBS for cell permeabilization, and then rinsed with PBS. The samples were stained by fluorescent dyes which render the F-actins (Alexa Fluor® 488 phalloid in, Invitrogen, CA, USA) and the nuclei (DAPI, Invitrogen, CA, USA) inside the cells, and then mounted by ProLong® gold anti-fade reagent.

2.8. Confocal laser-scanning microscopy

For multi-cellular architecture inside the 3D composite HA hydrogel fixed between a sigmacoted glass slide and a top covers lip, the confocal laser-scanning microscopy (Leica TCS SP2, Germany) was utilized to obtain the image sequences of VMC multi-cellular architecture in the vertical direction. An objective with a magnification of 10× and numerical aperture (N.A.) of 0.3 was used to primarily locate the area of interest within the sample, while an objective (HCX PL APO CS, OIL) of 40.0× and 1.25 N.A. was used during the imaging process. The Alexa Fluor® 488 phalloidin was detected upon excitation at 488 nm (40% laser line power set in AOTF) with an emission maxima around 520 nm through a band-pass filter. The pinhole size was 0.998 Airy. Hundreds of images were obtained in Z direction via the XYZ scan mode with scanning speed at 400 Hz. The Voxel-size is 0.732 (Width [μm]) × 0.732 (Height [μm]) × 1.000 (or 2.000) (Depth [μm]). The obtained image sequences were stacked and processed by the 3D reconstruction software Amira 5.2 Resolve RT (trial version), allowing precise volumetric visualization of the multi-cellular structure in 3D space, as well as efficient quantitative analysis of the structure.

3. Results and discussion

3.1. Hollow structure formation via cellular self-organization in composite hydrogels

We firstly investigated the cell viability for the VMCs. The results indicated that the cellular viability and proliferation have good performance in this study (Fig. 1), so that VMCs could form the self-organized structures. Additionally, the aspects on cytotoxicity and hydrogel degradation were discussed by the previous papers [15,18–20]. The cellular viability and proliferation have good performance in this study, so that VMCs could form self-organized structures.

The schematic diagrams of the experimental design are shown in Fig. 1A. VMCs, stem cell-like multi-potent cells with several remarkable capabilities for multi-cellular structure formation [21,22], was used as the cell model. The composite gels consist of two gels having distinct mechanical stiffness, connected with each other with a clear demarcation line to form a serrated interfacial surface between them (Fig. 2A).The hydrogel with different stiffness were synthesized by tuning the component proportion and measured by a plate-to-plate rheometer. Based on the measured mechanical moduli, GL′ and GL″ for lower-stiffness gel and GH′ and GH″ for and higher-stiffness gel, the difference in the magnitudes between GH′ and GL′ was confined within a particular range ($150 < GH' - GL' < 400$) according to our empirical tests for tubular structure formation. Note that VMCs were only encapsulated in the upper gel having lower stiffness at the initial time (Fig. 2A, the green dots denote the cells, and Fig. 2B). The width (Ws) and depth (ds) of the cell-laden slot were designed as 500 and 300 μm, respectively. The composite gel attached on the squared slide was placed into a size-matched petri dish (Fig. 2C, inset: the patterned lower gel part) and then covered by culture media.

In this composite hydrogel, cells spread and remarkably elongated after 24 h, and then migrated so that they began to aggregate around the interface on day 2 (Fig. 2D). The aggregation became more pronounced on day 4. Later, obvious big aggregates with a diameter of more than 100 μm along the interface line were observed on day 8 (Fig. 2D). At this time, the aggregates had already become a cylinder-like structure. The aggregates reached the maximum dimensions on day 10–12. The cylinder-like structure showed no significant further growth after day 11. The sample was fixed by 4% PFA on day 12.The fluorescent images of top view of the arrayed stand-up multi-cellular structure are shown in Fig. 2E (nuclei stained with DAPI) and the cross-sectional view of the multi-cellular structure at the middle position in length direction are shown in Fig. 2F (F-actin stained with phalloidin). Notably, in most cases, the multi-cellular structure and appeared as hollow shape and emerged around the interfacial planes. However, they may also grow around the corners (Fig. 2G) or the middle area between two adjacent interfaces (Fig. 2H). These dimensionally-large tubes have never been found in the common HA hydrogels without this composite structure, though large value ranges of synthesis parameters such as concentration of HA (2% to 5%), RGD (50 mM to 800 mM) and cross linkers (r = 0.3 to 0.8) have been tested.

The previous study reported that the HA polymers has a typical molecular weight over 10^6 daltons (Da), and they can be cleaved by the enzyme hyaluronidase (HAse) to obtain moleculars of much lower molecular weights [15]. Low molecular weight HA ($<3.5 \times 10^4$ Da) has been implicated as pro-inflammatory and pro-angiogenic. However, we have not paid full consideration for the function or effects of HAse (HA) in the tubular growth formation. Therefore, in the following study, we would explore the correlation between the hydrogels treating with HAse and HA and the tubular growth formation.

We next inspected the geometrical morphology of the self-organized 3D multi-cellular structures by confocal laser-scanning microscopy after the F-actins of cells stained by fluorescent dyes. Confocal laser-scanning microscopy verified that the multi-cellular aggregates had a hollow cavity, and revealed tube-like multi-cellular structures formed in HA hydrogel (Fig. 3). This multi-cellular tube had a continuous lumen (Fig. 3A–D). Also, each tube had one end covered and sealed by a dome shaped “lid”, which was a dense multi-cellular structure (Fig. 3A–D), and outer diameter larger than 150 μm, a wall thickness of 15–50 μm, and a length of more than 250 μm. In additional, the multi-cellular tubes in our experiments were approximately parallel to the vertical interfacial plane inside the composite gel (schematic elucidated in Fig. 3E,F). Here the dimensionally-large upright tube formed in 3D hydrogel is significantly different from the self-organized capillary-like tubal structures [16,17] as the diameters of the tubes formed in previous capillary-like tubes seemed always constrained within a

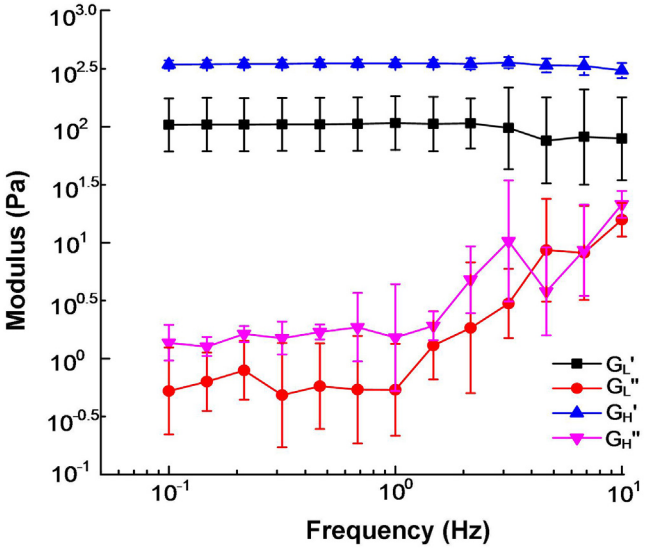

Fig. 5. The storage (G′) and loss modulus (G″) of the lower-stiffness gel (G_L' and G_L'') and higher-stiffness gel (G_H' and G_H'') (mean ± standard deviation; n = 5). The error bar is relative error bar, thus it is symmetrically plotted on the log (Modulus) scale.

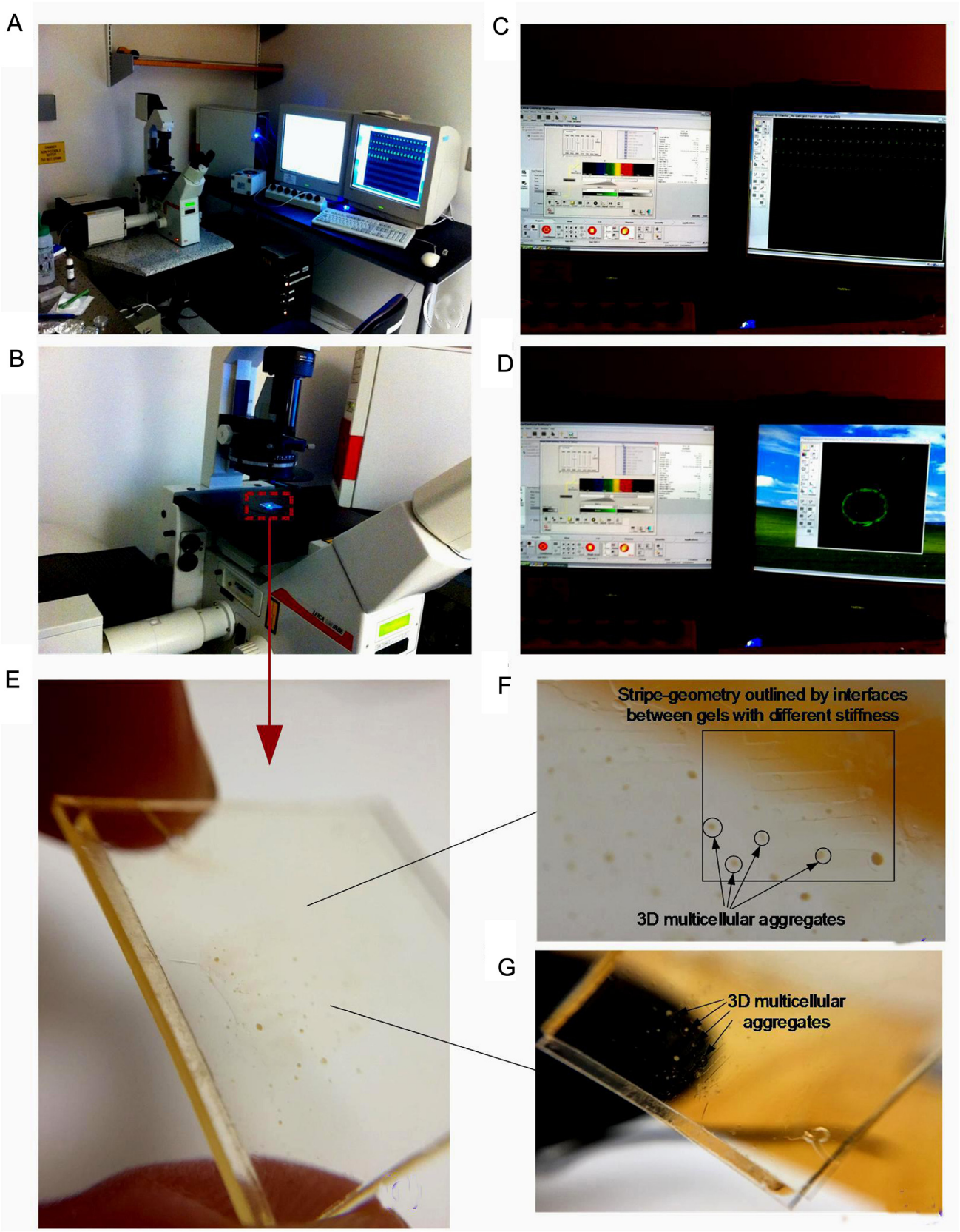

Fig. 6. The experimental images for confocal microscopy and the gross appearance of the small tubular structures with two capped ends. (A) The picture of the setup for confocal microscopy. (B) The composite HA hydrogel sheetsclamped by two glass slides were placed onto the stage of confocal microscope. (C and D) Scanning process for imaging the 3D multicellular structures inside composite hydrogel via confocal microscopy. (E) The gross appearance of the 3D multicellular aggregates with inside lumens after 12 days culture. The structures are tiny and the inside lumens can be detected via confocal microscopy as shown in (C and D) and the main text. (F and G) The local geometry of composite HA hydrogels and gross appearance of the 3D multi-cellular aggregates with inside lumens, whose central axes were approximately perpendicular to the glass slide surface, so the tubular structures cannot be easily found by eyes, but can be imaged by confocal microscopy.

single cell level. In contrast, here the diameter and length of this multi-cellular tube both strikingly exceed the single cell level. Fig. 3E,F summarized the generalized features for distribution of arrayed tubular structures and the location of each 3D tubular structure relative to the interfacial planes inside this hierarchical hydrogels. The vertical tubes (light pink color) are near the vertical interfaces of upper and lower gels. Each tube is constructed by a great number of cells, and the tubes usually partially invade into the higher-stiffness gel.

3.2. Quantitative characterization of the multi-cellular tube formation and the stiffness of hydrogels

We next sought to quantitatively characterize the tube formation in this cell-hydrogel system. The initial cell density encapsulated in the upper hydrogel with lower-stiffness is a critical factor affecting the number of the multi-cellular tubes (Nt) in the composite hydrogel. The cell density corresponding to the maximum Nt is around 5000 cells/μl (Fig. 4A). Lower cell density led to a decrease of both cell–cell interactions and signal molecules secreted by cells, which would gear down the cellular self-assembly progress. On the other hand, the higher cell density gives rise to the increased contact inhibition among adjacent cells when the culture becomes confluent by which cells restrict proliferation and cell division [21]. The geometrical scales of the multi-cellular tubes are impacted by several factors including the incubation duration (T) and depth of the cell-laden slot (ds) as show in Fig. 4B, C (the definition of ds is indicated in Fig. 4A). The self-formed tubes can grow larger over time, whereas they seem to stop growing after day 11. The tube length has a positive linear correlation with the depth of the cell-laden slots approximately.

The stiffness of hydrogels has also been evaluated and observed. The result indicated that the three dimensional tubular structure has been successfully established by observing the stiffness of hydrogels (Fig. 5). Actually, because of the differences of hydrogel stiffness, the hydrogel structural gradient was formed at the interface between the lower-stiffness gel and higher-stiffness gel. Therefore, the protein molecules formed the concentration gradient at crossing interface regions. Meanwhile, the cells also forms a concentration gradient at crossing interface regions. All of the above may be correlated with the formation of the tubular structure.

Furthermore, the gross appearance of the tubular structures after 12 days was also examined (Fig. 6A–D). The Fig. 6E–G may indicate the gross appearance of the 3D multi-cellular aggregates with inside lumens after 12 days culture. The structures are tiny and the inside lumens can be detected via confocal microscopy as shown in Fig. 6C and D. Fig. 6F and G showed the local geometry of composite HA hydrogels and gross appearance of the 3D multi-cellular aggregates with inside lumens, whose central axes were approximately perpendicular to the glass slide surface. Therefore, the tubular structures cannot be easily found by eyes, but can be imaged by confocal microscopy.

Although we obtained a few significant results, there were also some limitations. It is not surprising that the increase in stiffness at the interface is a barrier to cell penetration, providing impetus for self-aggregation. New knowledge on the defining range of stiffness for this to happen is however lacking. Due to the findings obtained from this study, we would investigate the profound and new knowledge in following study.

4. Conclusions

By using VMCs, we created 3D self-organized multi-cellular structures mimicking 3D features of tubular tissues. It demonstrates that 3D multi-cellular tubular structures can be derived by the self-organization of a single type of stem cells in rationally-devised composite hydrogels. These generated multi-cellular structures are proved to reveal a Turing-type mechanism based on the reaction-diffusion-advection of morphogens and cells. Mathematical models can rationally predict 3D multi-cellular tubular structure formation in a heterogeneous matrix according to the previous published report [24,25]. Modulating the dimensions of interfacial geometry, culture duration and cell density allow us to sculpt and pattern the evolving multi-cellular structures to generate tubular structures with various diameters and lengths. It lays a foundation for regenerating injured vasculatures in organs such as hearts, lungs, and kidneys more efficiently and at lower cost. This self-organization methodology based on Turing instability opens up new vistas for understanding and generating tubular tissues with an unprecedented level of rational controllability.

Conflict of interest

All authors declare no conflict of interest.

Acknowledgements

This work is supported by National Natural Science Foundation of China (Grant No. 51505127), Natural Science Foundation of Jiangsu Province (Grant No. BK20161197) and Fundamental Research Funds for the Central Universities (Grant No. 2015B04414) through Hohai University, China. This work was also supported in part by the NSF SINAM Center (UCB/NSF 00006047).

References

[1] K.A. Athanasiou, R. Eswaramoorthy, P. Hadidi, J.C. Hu, Self-organization and the self-assembling process in tissue engineering, Annu. Rev. Biomed. Eng. 15 (1) (2013) 115–136.
[2] X.K. Cao, R. Li, W. Sun, Y. Ge, B.L. Liu, Co-combination of islets with bone marrow mesenchymal stem cells promotes angiogenesis, Biomed. Pharmacother. 78 (1) (2015) 156–164.
[3] B. Lubarsky, M.A. Krasnow, Tube morphogenesis: making and shaping biological tubes, Cell 112 (1) (2003) 19–28.
[4] B. Yuan, Y. Jin, Y. Sun, D. Wang, J. Sun, Z. Wang, W. Zhang, X. Jiang, Artificial vessels: a strategy for depositing different types of cells in three dimensions to mimic tubular structures in tissues, Adv. Mater. 24 (7) (2012) 853-853.
[5] H. Onoe, T. Okitsu, A. Itou, M. Kato-Negishi, R. Gojo, D. Kiriya, K. Sato, S. Miura, S. Iwanaga, K. Kuribayashi-Shigetomi, Y.T. Matsunaga, Y. Shimoyama, S. Takeuchi, Metre-long cell-laden microfibres exhibit tissue morphologies and functions, Nat. Mater. 12 (6) (2013) 584–590.
[6] J.S. Miller, K.R. Stevens, M.T. Yang, B.M. Baker, D.H.T. Nguyen, D.M. Cohen, E. Toro, A.A. Chen, P.A. Galie, X. Yu, R. Chaturvedi, S.N. Bhatia, C.S. Chen, Rapid casting of patterned vascular networks for perfusable engineered three-dimensional tissues, Nat. Mater. 11 (9) (2012) 768–774.
[7] S.V. Murphy, A. Atala, 3D bioprinting of tissues and organs, Nat. Biotechnol. 32 (8) (2014) 773–785.
[8] H. Suga, T. Kadoshima, M. Minaguchi, M. Ohgushi, M. Soen, T. Nakano, N. Takata, T. Wataya, K. Muguruma, H. Miyoshi, S. Yonemura, Y. Oiso, Y. Sasai, Self-formation of functional adenohypophysis in three-dimensional culture, Nature 480 (1) (2011) 57–62.
[9] T. Takebe, K. Sekine, M. Enomura, H. Koike, M. Kimura, T. Ogaeri, R.R. Zhang, Y. Ueno, Y.W. Zheng, N. Koike, S. Aoyama, Y. Adachi, H. Taniguchi, Vascularized and functional human liver from an iPSC-derived organ bud transplant, Nature 499 (7459) (2013) 481–484.
[10] S.R. Franzdottir, I.T. Axelsson, A.J. Arason, O. Baldursson, T. Gudjonsson, M.K. Magnusson, Airway branching morphogenesis in three dimensional culture, Respir. Res. 11 (1) (2010) 162.
[11] W. Holnthoner, K. Hohenegger, A.M. Husa, S. Muehleder, A. Meinl, A. Peterbauer-Scherb, H. Redl, Adipose-derived stem cells induce vascular tube formation of outgrowth endothelial cells in a fibrin matrix, J. Tissue Eng. Regen. Med. 9 (2) (2015) 127–136.
[12] X. Zhu, H. Yang, In-silico constructing three-dimensional hollow structure via self-organization of vascular mesenchymal cells, The 16th International Conference on Nanotechnology (IEEE NANO 2016), August 22–25, 2016, Sendai, Japan, 2016, pp. 464–467 In press.
[13] T.H. Chen, J.J. Hsu, X. Zhao, C.Y. Guo, M.N. Wong, Y. Huang, Z.W. Li, A. Garfinkel, C.M. Ho, Y. Tintut, L.L. Demer, Left-right symmetry breaking in tissue morphogenesis via cytoskeletal mechanics, Circul. Res. 110 (2012) 551-U117.

[14] T.H. Chen, X. Zhu, L. Pan, X. Zeng, A. Garfinkel, Y. Tintut, L.L. Demer, X. Zhao, C. M. Ho, Directing tissue morphogenesis via self-assembly of vascular mesenchymal cells, Biomaterials 110 (4) (2012) 9019–9026.
[15] J. Lam, N.F. Truong, T. Segura, Design of cell-matrix interactions in hyaluronic acid hydrogel scaffolds, Acta. Biomater. 10 (4) (2014) 1571–1580.
[16] R. Sudo, S. Chung, I.K. Zervantonakis, V. Vickerman, Y. Toshimitsu, L.G. Griffith, R.D. Kamm, Transport-mediated angiogenesis in 3D epithelial coculture, FASEB J. 23 (7) (2009) 2155–2164.
[17] S.M. Anderson, S.N. Siegman, T. Segura, The effect of vascular endothelial growth factor (VEGF) presentation within fibrin matrices on endothelial cell branching, Biomaterials 32 (30) (2011) 7432–7443.
[18] Y. Lei, S. Gojgini, J. Lam, T. Segura, The spreading, migration and proliferation of mouse mesenchymal stem cells cultured inside hyaluronic acid hydrogels, Biomaterials 32 (1) (2011) 39–47.
[19] S. Gojgini, T. Tokatlian, T. Segura, Utilizing cell-matrix interactions to modulate gene transfer to stem cells inside hyaluronic acid hydrogels, Mol. Pharm. 8 (5) (2011) 1582–1591.
[20] J. Lam, T. Segura, The modulation of MSC integrin expression by RGD presentation, Biomaterials 34 (16) (2013) 3938–3947.
[21] N.G. Kim, E. Koh, X. Chen, B.M. Gumbiner, E-cadherin mediates contact inhibition of proliferation through Hippo signaling-pathway components, Proc. Natl. Acad. Sci. U. S. A. 108 (29) (2011) 11930–11935.
[22] K. Bostrom, K.E. Watson, S. Horn, C. Wortham, I.M. Herman, L.L. Demer, Bone morphogenetic protein expression in human atherosclerotic lesions, J. Clin. Invest. 91 (4) (1993) 1800–1809.
[23] P.K. Wong, F.Q. Yu, A. Shahangian, G.H. Cheng, R. Sun, C.M. Ho, Closed-loop control of cellular functions using combinatory drugs guided by a stochastic search algorithm, Proc. Natl. Acad. Sci. U. S. A. 105 (13) (2008) 5105–5110.
[24] M. Simunovic, C. Mim, T.C. Marlovits, G. Resch, V.M. Unger, G.A. Voth, Protein-mediated transformation of lipid vesicles into tubular networks, Biophys. J. 105 (3) (2013) 711–719.
[25] S. Berking, K. Herrmann, A model for tube formation and branching in Cnidaria, Central European Journal of Biology 5 (5) (2010) 710–723.